Materials Chemistry

Cite this: J. Mater. Chem., 2012, 22, 585

www.rsc.org/materials

PAPER

Biodegradable free-standing nanomembranes of conducting polymer:polyester blends as bioactive platforms for tissue engineering

Elaine Armelin,*[ab] Alex L. Gomes,[ac] Maria M. Pérez-Madrigal,[ab] Jordi Puiggalí,[ab] Lourdes Franco,[ab] Luis J. del Valle,[d] Alfonso Rodríguez-Galán,[a] João Sinézio de C. Campos,[c] Nuria Ferrer-Anglada[e] and Carlos Alemán*[ab]

Received 21st August 2011, Accepted 6th October 2011
DOI: 10.1039/c1jm14168f

The present study reports the fabrication of free-standing nanomembranes with semiconducting and biodegradable properties. Nanomembranes have been prepared by spin-coating mixtures of a semiconducting polythiophene derivative, poly(3-thiophene methyl acetate), and a biodegradable polyester, poly(tetramethylene succinate). Both the roughness and thickness of the nanomembranes, which ranged from 3 to 20 nm and from 20 to 80 nm, respectively, were precisely controlled through the spin-coater speed and the solvent evaporation properties. Nanomembranes made of conducting polymer/polyester blends, which are able to retain the properties of the individual polymers, are stable in air and in ethanol solution for more than one year, facilitating their manipulation. Enzymatic degradation essays indicated that the ultra-thin films are biodegradable due to the presence of the aliphatic polyester. Interestingly, adhesion and proliferation assays with epithelial cells revealed that the behavior of the blend as cellular matrix is superior to that of the two individual polymers, validating the use of the nanomembranes as bioactive substrates for tissue regeneration.

Introduction

Free-standing nanomembranes with macroscopic size and molecular scale thickness (*i.e.* size : thickness ratio greater than 10^6) are self-supporting substrates that combine properties of bulk materials along with individual properties.[1] This facilitates their macroscopic use in selected applications that require not only miniaturization in one dimension but also characteristics that are usually not compatible with conventional ultra-thin films: macroscopic robustness and homogeneity, nanoscale thickness, sufficient mechanical strength, flexibility, *etc.* Due to these unique technological characteristics, the preparation of nanomembranes has become a topic of growing interest.[1–9] In addition to their obvious interest as cell substrates for tissue engineering applications, robust membranes of macroscopic size and nanometric thickness could provide a unique family of drug-delivery vehicles, biomimetic systems, microfluidic valves, platforms for biosensors, wound dressing and even artificial organs. Within this context organic–inorganic hybrid nanomembranes ($\ell \approx 35$ nm) with an interpenetrating network structure deserve a special mention since the hybridization of cross-linked polymers (*e.g.* epoxy resins) with inorganic components (*e.g.* silica or zirconia) has been demonstrated to reinforce drastically the mechanical properties of the former materials.[1–5] Thus, these hybrid free-standing nanofilms are robust enough to hold amounts of liquid 7×10^4 times heavier than their own weight and are flexible enough to reversibly pass through holes 3×10^4 times smaller than their own size.

Ultrathin films based on conducting polymers (CPs), like polythiophene derivatives, or on mixtures of conventional insulating polymers and CPs have been reported to present semiconductor behavior, high environmental stability and good mechanical properties, opening a new route for the fabrication of organic nanotransistors for electronic devices.[6–9] Moreover, the application of CPs at the interface between biology and electronics has been found to be useful for the development of implants for tissue engineering[10,11] and nerve regeneration,[12] mechanical actuators (artificial muscles),[13] sensors,[14,15] *etc.* In recent studies we evidenced that CPs typically behave as a cellular matrix.[11,16] Thus, although the monomers used for their

[a]*Departament d'Enginyeria Química, E.T.S. d'Enginyers Industrials de Barcelona, Universitat Politècnica de Catalunya, Av. Diagonal 647, Barcelona, E-08028, Spain. E-mail: elaine.armelin@upc.edu; carlos.aleman@upc.edu*
[b]*Center for Research in Nano-Engineering, Universitat Politècnica de Catalunya, Campus Sud, Edifici C', C/Pasqual i Vila s/n, Barcelona, E-08028, Spain*
[c]*Departamento de Tecnologia de Polímeros, Faculdade de Engenharia Química, Universidade Estadual de Campinas, Avenida Albert Einstein no. 500, Barão Geraldo, CEP 13083-852 Campinas-SP, Brazil*
[d]*Departament d'Enginyeria Agroalimentària i Biotecnología, ESAB, Universitat Politècnica de Catalunya, C/Esteve Terradas 8, 08860 Castelldefels, Spain*
[e]*Departament de Física Aplicada, Universitat Politècnica de Catalunya, C/ Jordi Girona, 1-3, Barcelona, E-08034, Spain*

preparation are toxic for cells, the corresponding polymers are biocompatible materials with a relatively high content of salts (dopant ions) that promote the cell adhesion and proliferation. In spite of these interesting properties, the biomedical and biotechnological applications of CPs are limited yet. This should be mainly attributed to both their poor mechanical integrity and their lack of biodegradability.

The present work is focused on the fabrication of a new type of free-standing nanomembranes, which has been achieved by blending poly(3-thiophene methyl acetate) (P3TMA), a semiconducting polythiophene derivative, with poly(tetramethylene succinate) (PE44), a biodegradable polyester. The major achievements of this study can be summarized as follows: (i) P3TMA:PE44 blends retain the semiconducting properties of P3TMA and the biodegradability of PE44; (ii) polyester matrices are good supports for CPs since they provide mechanical integrity to the latter; and (iii) P3TMA:PE44 free-standing nanomembranes enhance the cell adhesion and proliferation behavior with respect to the individual homopolymers. Both the biodegradability and the excellent behavior as cellular substrates of P3TMA:PE44 nanomembranes allow us to conclude that they should be considered as promising bioactive platforms for tissue engineering applications.

Experimental

Materials

3-Thiophene acetic acid (3TAA, 98.0%), poly(4-hydroxysytrene) (PHS, M_w *ca.* 11 000), magnesium sulfate (97+%), 1,4-butanediol (99.0%), succinic acid (≥99.0%) and titanium(IV) butoxide (97%) were purchased from Sigma-Aldrich, Germany. Iron(III) chloride anhydrous (97.0%), methanol (99.5%), ethanol (99.5%), diethyl ether stabilized with 6 ppm of BHT-QP (99.5%), trichloromethane dry stabilized with 50 ppm of amylene DS-ACS (99.9%) and sulfuric acid (98.0%) were purchased from Panreac Quimica S.A.U. (Spain). Dichloroacetic acid solution (≥99.0%) used for intrinsic viscosity characterization and 1,1,1,3,3,3-hexafluoro-2-propanol (≥99.8%) used for size exclusion chromatography were both purchased from Sigma-Aldrich, Germany. All reagents were used as received without further purification.

For cell culture experiments, human laryngeal epidermoid carcinoma cells (HEp-2) were purchased from ATCC (USA). Dulbecco's phosphate buffered saline (PBS) solution without calcium chloride and magnesium chloride, Dulbecco's modified Eagle's medium (DMEM, with 4500 mg of glucose per L, 110 mg of sodium pyruvate per L and 2 mM of L-glutamine), penicillin–streptomycin, 3-(3,5-dimethylthiazol-2-yl)-2,5-diphenyl-2*H*-tetrazolium bromide (MTT, 97.5%) and trypsin–EDTA solution (0.05% trypsin, 0.02% EDTA) were all purchased from Sigma, Germany. Fetal bovine serum (FBS) and trypan blue stain (0.4%) were purchased from Gibco, UK. Dimethyl sulfoxide (99.0%) was purchased from Panreac Quimica S.A.U. (Spain) and sodium azide (NaN_3, ≥99.5%) from Sigma-Aldrich, Germany. Finally, lipase F-Ap15 (from *Rhizopus oryzae*) was purchased from Sigma, Germany, and used in the enzymatic degradation analyses.

Synthesis of poly(3-thiophene methyl acetate)

Using 3TAA as starting monomer and $FeCl_3$ as oxidant, 3-thiophene methyl acetate (3TMA) was prepared and subsequently polymerized by oxidative coupling following the procedure described by Osada and co-workers.[17] The purified 3TMA monomer was obtained with 82% yield, while the yield of P3TMA was 25% after removal of the residual oxidant and oligomers. Unfortunately, changes in the 3TMA : $FeCl_3$ ratio did not improve the low yield of the oxidative coupling polymerization. The FTIR and ^{1}H-NMR characterizations of the produced P3TMA (not shown) were in complete agreement with those previously reported.[17]

Synthesis of poly(tetramethylene succinate)

The biodegradable polyester was prepared by bulk thermal polycondensation of 1,4-butanediol and succinic acid (diol/diacid molar ratio of 2.2/1).[18] The reaction was first performed in a nitrogen atmosphere at 150 °C for 6 hours and then in vacuum at 180 °C for 18 hours. Titanium tetrabutoxide was used as a catalyst. The polymer was dissolved in chloroform and precipitated with ethanol. PE44 was obtained with a 72% yield after drying overnight under vacuum.

Viscosity and molecular weights

The intrinsic viscosity of PE44, 0.80 dL g^{-1}, was determined using a Cannon-Ubbelohde microviscometer and a dichloroacetic acid solution at 25 ± 0.1 °C. The intrinsic viscosity of P3TMA was not evaluated due to the insolubility of this material in dichloroacetic acid.

Molecular weights were estimated by size exclusion chromatography using a liquid chromatograph (Shimadzu, model LC-8A) equipped with an Empower computer program (Waters). A PL HFIP gel column (Polymer Lab) and a refractive index detector (Shimadzu RID-10A) were employed. Polymers were dissolved and eluted in hexafluoroisopropanol at a flow rate of 0.5 mL min^{-1} (injected volume 100 μL, sample concentration 1.5 mg mL^{-1}) and using poly(methyl methacrylate) standards. The resulting number and weight average molecular weight were [$\overline{M_n}$ = 10 500 g mol^{-1} and $\overline{M_w}$ = 22 500 g mol^{-1}] and [$\overline{M_n}$ = 24 365 g mol^{-1} and $\overline{M_w}$ = 36 524 g mol^{-1}] for PE44 and P3TMA, respectively.

Preparation of free-standing nanomembranes

The procedure described by Kunitake and co-workers[4,5] for the preparation of ultrathin films of epoxy resins has been followed in this work for the fabrication of P3TMA:PE44 nanomembranes. Poly(4-hydroxystyrene) in ethanol (5 wt%) was firstly spin-coated on an indium-tin oxide (ITO) glass slide (dimensions ranged from 2.5 × 2.5 to 5.0 × 10.0 cm^2) at 3000 rpm for 60 s to give a 0.1 mm thick sacrificial layer after two applications. On the other hand, sonicated powder of P3TMA and PE44 were separately dissolved in chloroform and then mixed. The resulting mixtures, which were prepared considering 80 : 20, 50 : 50 and 20 : 80 molar ratios, were subsequently stirred at room temperature for 10 minutes. The dispersions were then diluted with chloroform (dilution ratio: 1 : 5), filtered and subjected to spin-coating for film deposition. The thickness of the films was adjusted in the range of 15–100 nm by varying the spin-coater speed (from 1500 to 8000 rpm). After coating, the samples were immersed into ethanol for the nanomembrane separation

from the ITO substrate. The edge of the specimens was cut to help penetration of ethanol into the sacrificial layer.

Thermal analyses

Calorimetric data were obtained by differential scanning calorimetry (DSC) with a TA Instruments Q100 series equipped with a refrigerated cooling system (RCS) operating at temperatures from −90 °C to 600 °C. Experiments were conducted under a flow of dry nitrogen with a sample weight of approximately 5 mg, calibration being performed with indium. The T_{zero} calibration requested two experiments: the first was done without samples while the second one was performed with sapphire disks. Hot crystallizations were performed at a cooling rate of 10 °C min^{-1} with melted samples previously heated until 200 °C to erase the thermal history. Heating runs were performed at 20 °C min^{-1} with samples previously quenched from the melt state by cooling at the maximum rate allowed by the equipment. Determination of T_g values from the calorimetric curves was carried out with the TA-Universal Analysis software furnished with the instrument. Thermal degradation was determined at a heating rate of 20 °C min^{-1} with around 5–8 mg samples in a Q50 thermogravimetric analyzer of TA Instruments and under a flow of dry nitrogen. The analysis was performed in the temperature range from 30 °C to 800 °C. For polymer kinetic analysis additional heating scans were carried out at rates ranging from 5 °C min^{-1} to 20 °C min^{-1}. In all cases deconvolution of the derivative thermogravimetric curves was performed with the PeakFit v4 program by Jandel Scientific Software using an asymmetric double sigmoidal function.

Microscopy studies

Optical microscopy observations were performed using a Zeiss Axioskop 40 Pol light polarizing microscope equipped with a Linkam temperature control system configured by a THMS 60. Micrographs were taken with a Zeiss AxiosCam MRC5 digital camera. A first-order red tint plate was employed to determine the sign of spherulite birefringence under crossed polarizers.

Scanning electron microscopy (SEM) studies were carried out using a Focused Ion Beam Zeiss Neon40 scanning electron microscope equipped with an energy dispersive X-ray (EDX) spectroscopy system and operating at 30 kV. Samples were mounted on a double-sided adhesive carbon disc and sputter-coated with a thin layer of carbon to prevent sample charging problems.

Atomic force microscopy (AFM) was employed to take topographic images of P3TMA:PE44 nanomembranes. Images were obtained with a Molecular Imaging PicoSPM using a NanoScope IV controller under ambient conditions. The tapping mode AFM was operated at constant deflection (*i.e.* vertical constant force with triangular shaped gold-coated silicon nitride). The row scanning frequency was set to 1 Hz and the physical tip-sample motion speed was 10 μm s^{-1}. The RMS roughness (r) was determined using the statistical application of the Nanoscope software, which calculates the average considering all the values recorded in the topographic image with the exception of the maximum and the minimum. The scan window size was 5 × 5 μm^2 in all cases, a total of 65 536 topographic data points being computed in each image.

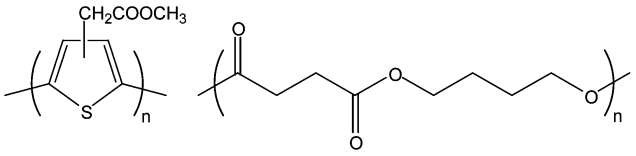

P3TMA **PE44**

Scheme 1 Chemical structures of poly(3-thiophene methyl acetate), P3TMA, and poly(tetramethylene succinate), PE44.

Conductivity measurements

In order to measure the electrical properties, films of P3TMA:PE44 were spin-cast onto glass substrates from 10 wt% $CHCl_3$ solutions, and dried under vacuum overnight. The nanofilms (thickness from 20 to 80 nm) were partially coated with silver paint to yield two electrodes for two-probe conductivity measurements. A direct voltage ranging from −20 to +20 V was applied, the current response being measured with a Keithley 6430 Sub-FemtoAmp Remote Sourcemeter. Conductivity (σ) was calculated as $\sigma = LR^{-1}A^{-1}$, where L (cm) is the distance between the electrodes, R (Ω) is the membrane resistance, and A (cm^2) is the cross-sectional area of the membrane.

Enzymatic degradation studies

Ultrathin films were prepared by extending 20 μL of polymer solution in a steel sheet of 1 cm^2 and spin-coating at 1000 rpm for 30 s. The films were placed in Petri dishes containing Lipase PS 4 mg mL^{-1} (from *Rhizopus oryzae*, Sigma Aldrich 80612) in 10 mL of phosphate buffer solution (pH 7.4) supplemented with 0.1 mg mL^{-1} of sodium azide, and incubated at 37 °C for one and four weeks. The enzymatic solution was replaced every 48 h. After each incubation period, samples were removed from the enzymatic solution, and washed thoroughly with distilled water. After wiping, specimens were dried under vacuum at room temperature. Biodegradation was evaluated by optical microscopy and SEM. For SEM studies, samples were sputter-coated with carbon before observation.

Cellular adhesion and proliferation studies

PE44, P3TMA and P3TMA:PE44 nanomembranes were prepared and deposited by solvent casting on steel pieces of 1 cm^2. Human laryngeal epidermoid carcinoma (HEp-2) cells were cultured in Dulbecco's modified Eagle medium (DMEM

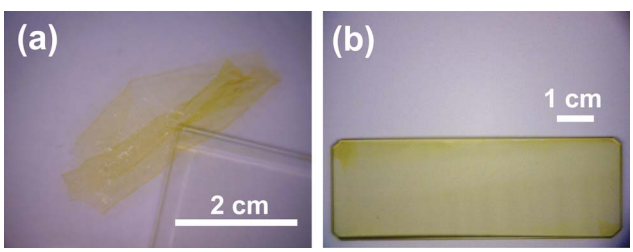

Fig. 1 Digital camera images of a P3TMA:PE44 free-standing nanomembrane (a) dispersed in ethanol (*i.e.* after removal from ITO) and (b) deposited on a glass substrate (*i.e.* after removal from ITO, the nanomembrane was re-deposited).

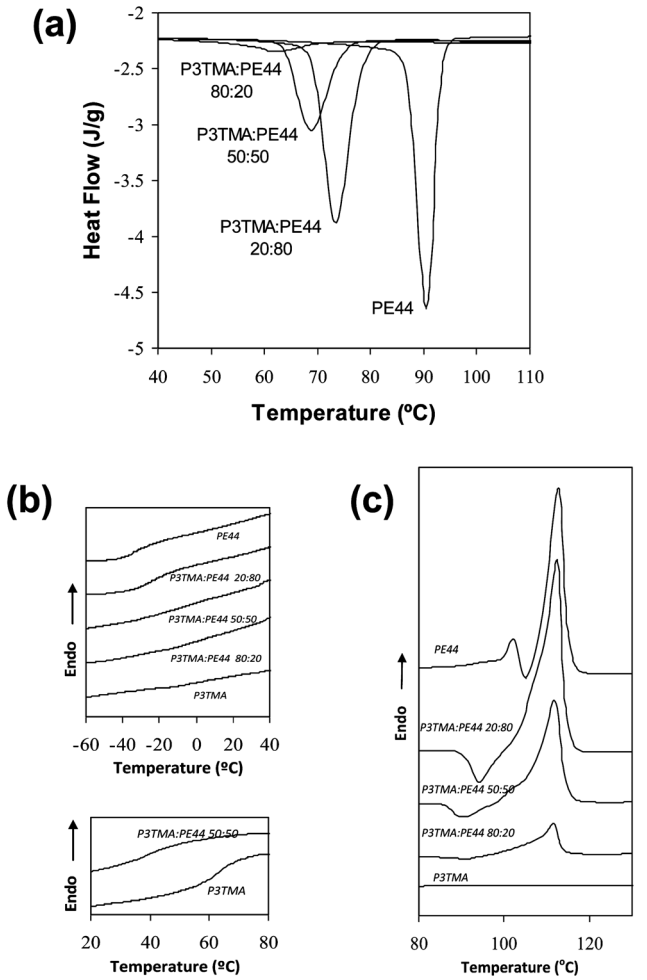

Fig. 2 (a) Dynamic DSC curves (10 °C min^{-1}) showing the exothermic crystallization peak of the different P3TMA:PE44 samples. (b) DSC heating traces (20 °C min^{-1}) showing the glass transitions associated with PE44 (up) and P3TMA (down) domains for the indicated blends. (c) DSC heating traces (20 °C min^{-1}) showing the melting behaviour of the indicated P3TMA:PE44 blends.

high glucose) supplemented with 10% fetal bovine serum, penicillin (100 units per mL), and streptomycin (100 μg mL^{-1}) at 37 °C in a humidified atmosphere of 5% CO_2 and 95% air. The culture media were changed every two days. When the cells reached 80–90% confluence, they were detached using 1–2 mL of trypsin/EDTA (0.05% and 0.02%, respectively) and centrifuged at 650*g* for 1 min. Finally, the cells were re-suspended in fresh media, the concentration of cells being determined by counting at the Neubauer camera using 4% trypan blue as dye vital.

Cells were seeded onto the nanomembranes and placed in plates of 24 wells. Previously, the steel substrates coated with the nanomembranes were placed in the wells and sterilized by UV-light for 15 min in a laminar flux cabinet. Aliquots of 50 μl containing 5×10^4 cells (for adhesion assay) or 2×10^4 cells (for proliferation assay) were deposited onto nanomembranes. The plate was incubated under culture conditions for 60 min to allow cell attachment to the material surface. Finally, 1 mL of the culture medium was added to each well. The controls of adhesion and proliferation were obtained by culturing cells on the surface of the tissue culture polystyrene (TCPS) plates and steel sheets.

Cell adhesion was evaluated by the MTT assay[19] carried out after 24 h of culture. Cell proliferation was also evaluated by MTT after 7 days of culture. The viability results were normalized to TCPS control as relative percentages. Five replicates for each independent experiment were averaged and graphically represented. ANOVA and Tukey's test were performed as statistical analysis at a confidence level of 95% ($p < 0.05$).

After culture, the sample were fixed in 2.5% glutaraldehyde–PBS overnight at 4 °C, then dehydrated by washing in an alcohol battery (30°, 50°, 70°, 90°, 95° and 100°) at 4 °C for 30 min per wash. Finally, the samples were dried and covered by carbon sputtering for examination by SEM.

Results and discussion

Polymer synthesis and nanomembrane fabrication

Many technological applications of organic CPs are seriously limited by their poor mechanical properties. Thus, many strategies to improve the mechanical integrity of these interesting materials have been proposed in the last few years. In this work, we have prepared P3TMA:PE44 nanomembranes not only to enhance the mechanical integrity of this conducting polymer but also to promote its use in biomedical applications. Specifically, the electron-withdrawing carboxylate groups of P3TMA (Scheme 1) have increased both the environmental stability and the solubility of the polythiophene, while the polyester matrix has provided mechanical integrity and biodegradability. The combination of these properties allows us to propose the use of P3TMA:PE44 as a new material with interesting biomedical applications.

P3TMA is highly soluble in chloroform, this behavior being also showed by other polythiophenes bearing carboxylate substituents in the 3-position of the thiophene ring.[20–23] The Hildebrand solubility parameter of PE44,[18] which is also soluble

Table 1 Calorimetric data of P3TMA:PE44 blends[a]

Sample	T_c/°C	ΔH_c[b]/J g^{-1}	T_{g1}/°C	T_{g2}/°C	w_1[c]	w_2[d]	T_f/°C
PE44	93.2	75.0	−34	—	100	0	102, 112.8
P3TMA:PE44 20 : 80	73.5	73.8	−27	—	0.89	—	112.5
P3TMA:PE44 50 : 50	68.8	66.5	−20	38	0.79	0.89	111.8
P3TMA:PE44 80 : 20	62.0	33.4	−10	45	0.65	0.96	111.6
P3TMA	—	0	—	63	0	100	—

[a] Cooling and heating runs performed at 10 and 20 °C min^{-1}, respectively. [b] Referred to the PE44 content. [c] PE44 weight fraction in the PE44 phase. [d] P3TMA weight fraction in the P3TMA phase.

in chloroform, is expected to be similar to that of P3TMA suggesting a partial miscibility between them. Thermal polycondensation of 1,4-butanediol and succinic acid yielded a polyester with high polydispersity (PD = 2.14) whereas the oxidative polymerization produced a CP with uniform size and almost homogeneous distribution (PD = 1.50). Therefore, P3TMA exhibits a stabilizing effect in the blend formation, avoiding the coagulation and agglomeration of P3TMA in the polyester matrix. In this sense, different segments of PE44 absorb P3TMA particles through attractive forces, resulting in a homogeneous distribution of nanoparticles (see the next section). P3TMA:PE44 nanomembranes with 80 : 20, 50 : 50 and 20 : 80 molar ratios were prepared by spin-coating using an ITO substrate and a poly(4-hydroxystyrene) sacrificial layer (see the Methods section). The resulting free-standing nanomembranes (Fig. 1a and b), which were detached from the substrate by dissolving the sacrificial layer, are flexible ultra-thin films with average thicknesses and areas ranging from ~20 to ~80 nm and from 4 to 50 cm^2, respectively. The thickness is controlled through both the speed applied to the spin-coater and the blend composition, while the area depends on the dimensions of the substrate. The nanomembranes are stable in air and in ethanol solution for their manipulation, such stability remaining more than a year after their preparation.

Thermal analyses

Calorimetric data reveal that P3TMA and PE44 are partially miscible. Specifically, DSC cooling runs from the melt state (Fig. 2a) indicate that the crystallization of PE44 is hindered by the presence of P3TMA. Thus, both the temperature of the exothermic crystallization peak and the crystallization enthalpy decrease when the P3TMA content increases (Table 1). Heating runs of melt quenched samples show two glass transition temperatures (T_g), as expected from a phase separation (Fig. 2b). Values corresponding to each phase were determined separately. It was clearly found that the determined glass transition temperatures depend on the composition, evidencing a partial miscibility. The T_g associated with the P3TMA decreases with the concentration of this polymer in the blend, while the T_g of PE44 increases when the concentration of polyester in the blend decreases (Table 1). The weight percentage of each polymer in the corresponding phase was determined from eqn (1) (Table 1):

$$\frac{1}{T_g} = \frac{w_1}{T_{g,1}} + \frac{w_2}{T_{g,2}} \quad (1)$$

where $T_{g,1}$ and $T_{g,2}$ correspond to the T_g of the pure components (*i.e.* −34 °C and 63 °C for PE44 and P3TMA, respectively) and, w_1 and w_2 are the weight fractions in the studied phase.

On the other hand, the fusion of the PE44 crystalline fraction is also affected by the incorporation of P3TMA (Fig. 2c). The polyester has two well defined melting peaks that have been associated with the existence of two populations of lamellar crystals with different thickness.[24] The first peak corresponds to the melt of thinner crystals, which undergo a reorganization giving rise to the intermediate exothermic peak. This melt/reorganization process is less clear in the heating runs of the studied blends, the first melting process being only detected as a small shoulder of the main peak. Heating traces of all blends show also

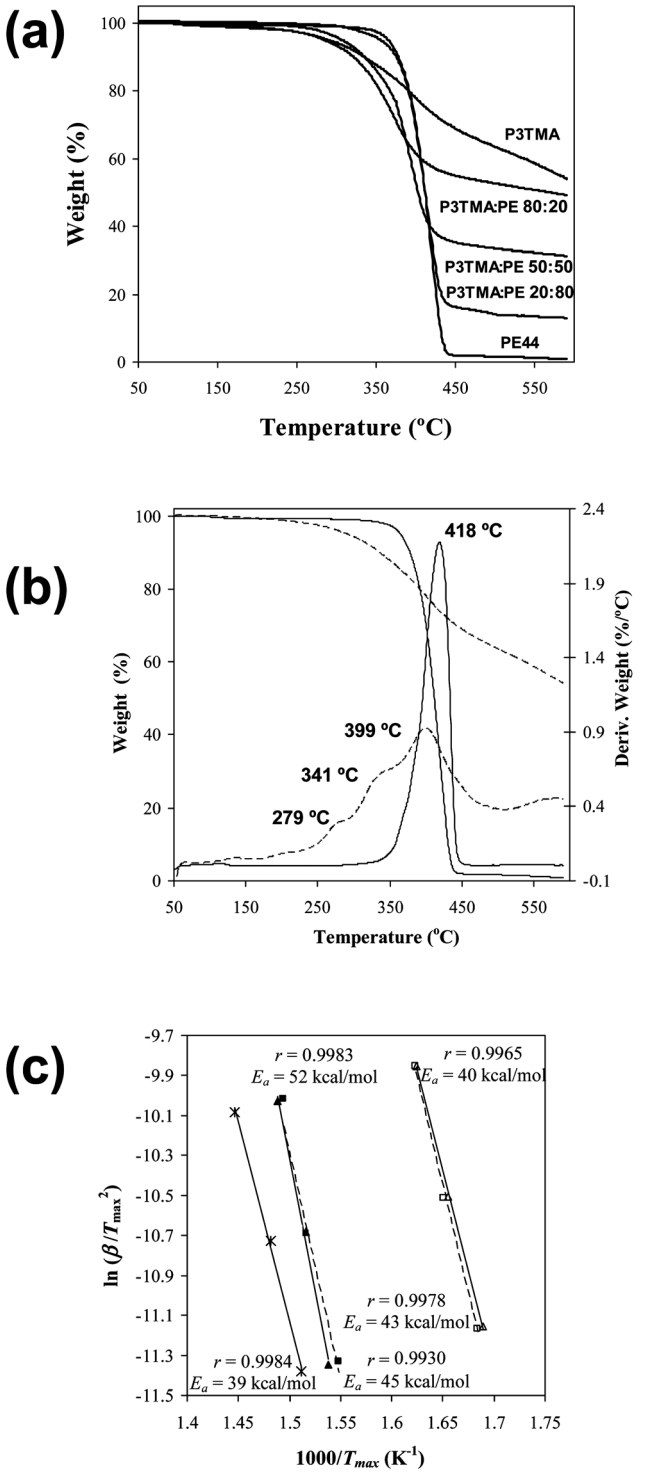

Fig. 3 (a) Thermogravimetric curves obtained at a heating rate of 20 °C min^{-1} for the P3TMA:PE44 blends and the two individual polymers. (b) Derivative thermogravimetry curves corresponding to the thermal decomposition of PE44 (solid lines) and P3TMA (dashed lines) polymers. (c) Kissinger plots for the thermal decomposition of PE44 (*) and the two main thermal decomposition steps observed for P3TMA (solid lines, ▲ symbols) and P3TMA:PE44 50 : 50 (dashed lines, ■ symbols) samples. Full and empty symbols correspond to the peaks appearing at the highest and the intermediate temperature, respectively.

Table 2 Thermogravimetric data of P3TMA:PE44 blends[a]

Sample	T_{onset}/°C	$T_{20\%}$[b]/°C	$T_{50\%}$[b]/°C	$T_{70\%}$[b]/°C	T_{max}/°C		
PE44	390	392	412	421	418		
P3TMA/PE44 20 : 80	385	391	412	424	415	321	
P3TMA/PE44 50 : 50	357	368	403	—	396	344	284
P3TMA/PE44 80 : 20	320	355	572	—	373		282
P3TMA	314	391	—	—	399	341	279

[a] Heating rate of 20 °C min^{-1}. $T_{20\%}$, $T_{50\%}$ and $T_{70\%}$ correspond to the temperatures after 20%, 50% and 70% degradation, respectively.

a small cold crystallization exothermic peak around 95 °C (*i.e.* before any fusion process). Finally, the melting peak of the thicker crystals slightly decreases when the content of P3TMA increases (Table 1). However, shifts are lower than 2 °C in all cases, evidencing that the contamination of PE44 crystals is very low.

Thermogravimetric scans show that the onset degradation temperature and the temperature corresponding to a given weight loss increase with the content of PE44 (Fig. 3a). Table 2 indicates that the thermal stability of the blends is highly dependent on the P3TMA:PE44 composition (*i.e.* PE44 increases the thermal stability of P3TMA and decreases the char yield, which reaches practically constant values at 500 °C). Nevertheless, although the incorporation of P3TMA decreases the thermal stability of the aliphatic polyester, the blends are very stable with degradation temperatures ranging between 320 and 385 °C.

The derivative thermogravimetry (DTG) curve of PE44 shows a single peak (418 °C) while the curve corresponding to the conducting polymer was characterized by three well differentiated shoulders (399, 341 and 279 °C), indicating a complex degradation behavior (Fig. 3b). DTG curves of PE44:P3TMA blends (Table 2) also revealed complex behavior, which depends on the polymers ratio in the mixture. However, it is interesting to note that the blend with an intermediate composition (50 : 50) showed three DTG shoulders at temperatures close to those determined for P3TMA (Table 2). These results suggest that the degradation of P3TMA gives rise to radicals that favor the decomposition of the aliphatic polyester, the DTG shoulder of the latter appearing at practically the same temperature as that of the main decomposition step of P3TMA.

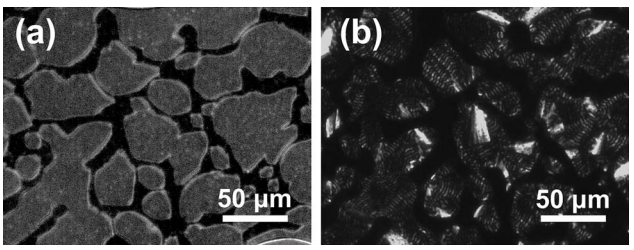

Fig. 4 Optical micrographs of P3TMA/PE44 50 : 50 (a) in the melt state and (b) after isothermal crystallization at 70 °C, black domains corresponding to the P3TMA phases.

DTG curves obtained at different heating rates (5, 10 and 20 °C min^{-1}) were used to estimate the activation energies, E_a, associated with the single degradation step of PE44 and the two main decomposition steps of the individual P3TMA and the P3TMA:PE44 blend with a 50 : 50 molar ratio. For this purpose, the Kissinger method[25] was applied because of its simplicity:

$$\ln \frac{\beta}{T_{max}^2} = \ln \frac{AR}{E_a} + \ln \left[n(1-\alpha_{max})^{n-1} \right] - \frac{E_a}{RT_{max}} \quad (2)$$

where β is the heating rate, T_{max} is the temperature at the maximum reaction rates associated with each degradation step, α_{max} is the conversion at this T_{max} temperature, n is the reaction order and A is the frequency factor.

The representation of $\ln \beta/T_{max}^2$ against $1/T_{max}$, which was fitted to a straight line using a simple linear regression, allowed us to determine the E_a from the slope of the resulting linear equation. It should be noted that this method is a rough approximation since it is not a rigorous isoconversional method. Thus,

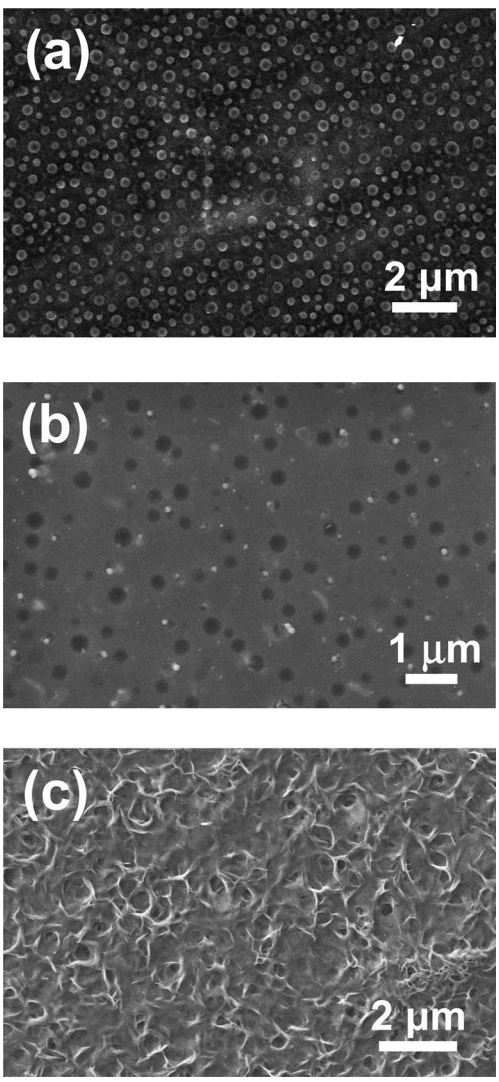

Fig. 5 SEM micrographs of nanomembranes made of: (a) P3TMA:PE44 blend with a 50 : 50 molar ratio, (b) individual P3TMA, and (c) individual PE44.

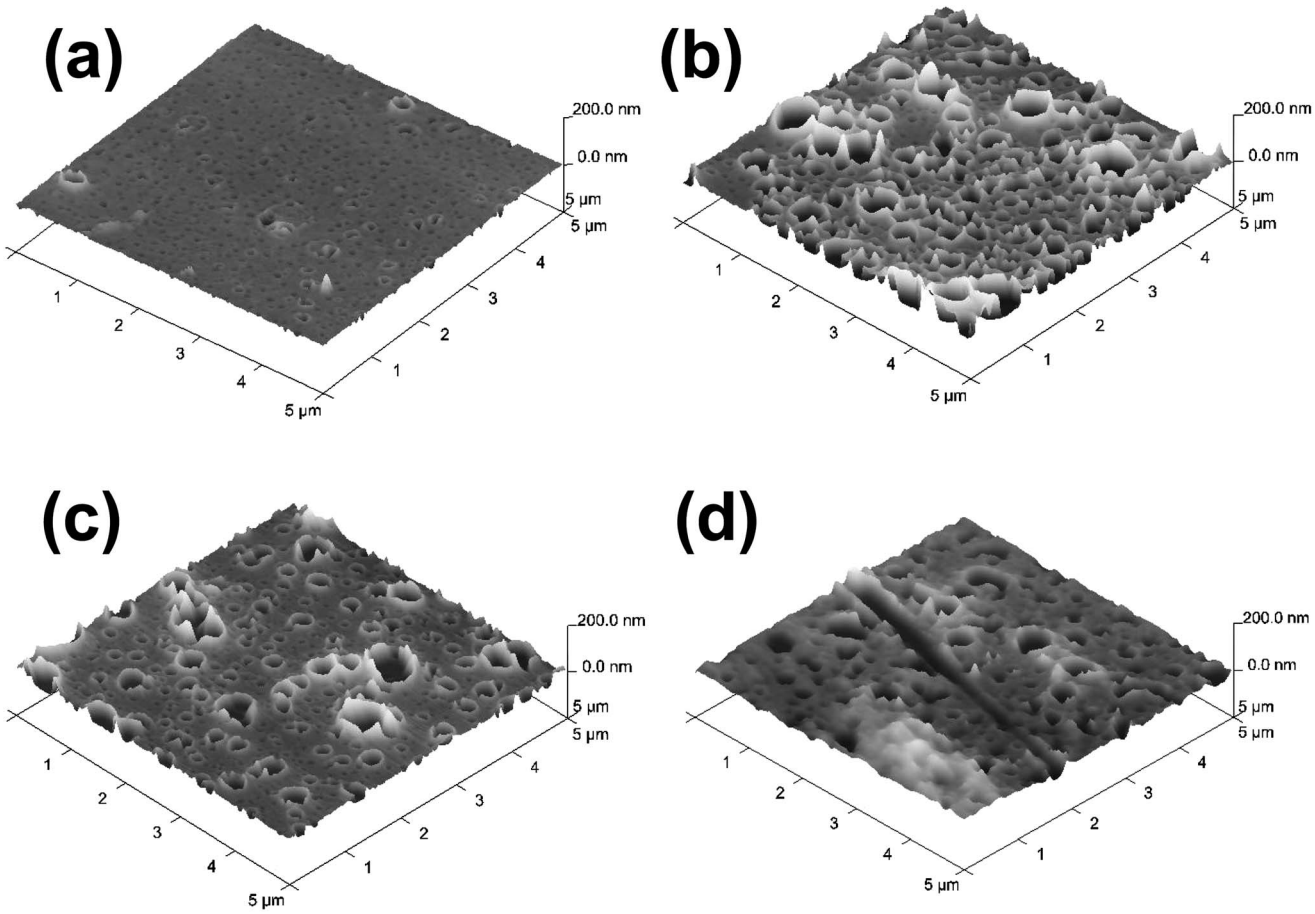

Fig. 6 3D AFM images of the nanomembranes prepared using the P3TMA:PE44 50 : 50 blend and spin-coating for 60 s at a speed of: (a) 3000 rpm; (b) 1500 rpm; (c) 5000 rpm; and (d) 8000 rpm. The thickness of the films was determined using AFM scratch, an example of scratch being displayed in (d).

the peak temperature of each step is obtained at different heating rates, and the extent of conversion related to a given peak is known to change with the heating rate.[26,27] Moreover, the determined activation energies may lose sense if they vary throughout the degradation processes.

Fig. 3c shows the Kissinger plots of the thermal decomposition steps of the three investigated samples. The linear plot of PE44, which showed the lowest activation energy ($E_a = 39 \pm 2$ kcal mol^{-1}), was clearly shifted to the high temperature zone, whereas the two main decomposition steps of the 50 : 50 blend and the P3TMA samples provided very similar linear plots. In spite of this, the highest activation energy ($E_a = 52 \pm 3$ kcal mol^{-1}) was determined for the high temperature decomposition step of P3TMA, the activation energy of the equivalent decomposition step of the 50 : 50 P3TMA:PE44 blend ($E_a = 45 \pm 4$ kcal mol^{-1}) being half way between those of individual PE44 and P3TMA. Finally, the activation energies for the second decomposition step of the 50 : 50 blend and the individual P3TMA were practically identical ($E_a = 43 \pm 3$ and 40 ± 1 kcal mol^{-1}, respectively).

Microscopy studies

Optical micrographs of melted blends showed a phase separation, suggesting again a partial miscibility, which after keeping the samples at 70 °C became the amorphous and crystalline domains of P3TMA and PE44, respectively (Fig. 4). Typical double ringed spherulites of PE44 were developed during these isothermal crystallizations. The P3TMA amorphous phase corresponds to the black domains in Fig. 4. As it can be seen, the amorphous domains of P3TMA tend to preclude the formation of spherulites by the crystalline phases of PE44. Accordingly, the amount of double ringed spherulites on blends decreases when the concentration of CP increases.

SEM images indicated a completely homogeneous distribution of the P3TMA and PE44, as is evidenced in Fig. 5a for the nanomembrane with a 50 : 50 molar ratio. According to the sulfur concentration detected by EDX spectroscopy, the embedded spherical nanoaggregates shown in such a micrograph correspond to the P3TMA trapped in the polyester matrix. Comparison of the SEM micrographs obtained for the 20 : 80, 50 : 50 and 20 : 80 nanomembranes (20 : 80 and 80 : 20 not shown) indicates that the number of spherical nanoaggregates increases with the concentration of CP, even though their distribution was homogeneous in all cases. SEM micrographs of P3TMA, like that displayed in Fig. 5b, also evidence spherical nanoaggregates of small (40–70 nm) and medium (250–340 nm) size. Thus, P3TMA does not present good film-forming properties, bigger particles detaching from the polymer surface. However, good mechanical integrity is obtained by blending the CP with PE44. On the other hand, PE44 nanomembranes

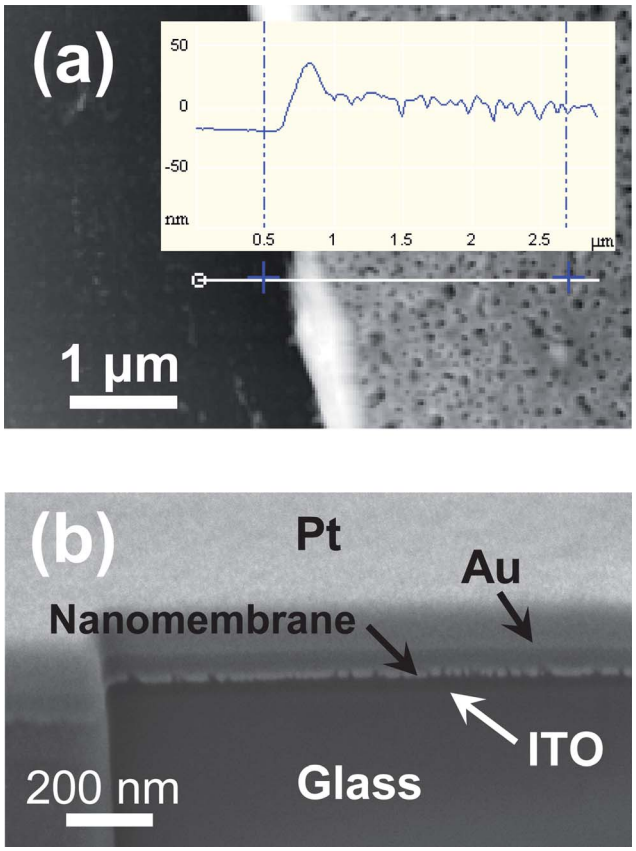

Fig. 7 Thickness of the 50 : 50 nanomembrane obtained using a spin-coater speed of 3000 rpm for 60 s determined using (a) the AFM scratch (the topographic image and the corresponding height profile are displayed as the inset) and (b) the SEM micrograph of a cross-sectional nanomembrane (the different material layers are displayed).

showed lamellar aggregates with superficial porosity, as is clearly reflected in Fig. 5c. The porosity induced by these microstructures is expected to facilitate the blending between the polyester and the CP.

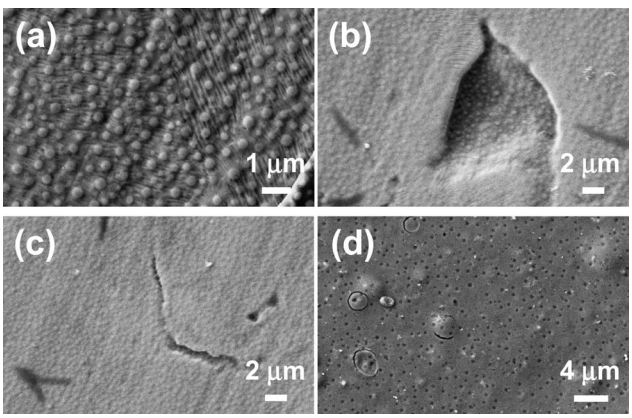

Fig. 8 SEM micrographs of the 50 : 50 nanomembrane after (a) one week and (b and c) three weeks of exposure under enzymatic degradation conditions. (d) SEM micrograph of an ultrathin film of P3TMA after four weeks of incubation in the enzymatic medium.

The topography of the nanofilms depends on the speed used in the spin-coating process. The 3D AFM image of the 50 : 50 nanomembrane deposited on a silicon wafer substrate using 3000 rpm (Fig. 6a) shows a very smooth surface with some small pores randomly distributed. The measured RMS roughness ranged from 3 to 5 nm, this value being similar to that typically measured for the ITO substrate (~4 nm). The number and size of the pores, as well as the RMS roughness, are significantly higher for the nanomembranes prepared using smaller (1500 rpm) and larger (5000 and 8000 rpm) spin-coater speeds. More specifically, the RMS roughness determined for the 1500, 5000 and 8000 rpm samples ranges within the following intervals: from 16 to 20 nm (Fig. 6b), from 10 to 11 nm (Fig. 6c), and from 12 to 13 nm (Fig. 6d), respectively.

The thickness of the films was determined using AFM scratch, an example of a scratch being displayed in Fig. 6d. The average thickness determined by AFM scratch (Fig. 7a) of the nanomembranes produced using 3000 rpm is $\ell = 15$ nm, this value increases to $\ell = 71$, 62 and 55 nm for 1500, 5000 and 8000 rpm, respectively. Thus, 3000 rpm has been found to be the optimum speed to produce 50 : 50 nanofilms with the smallest roughness and thickness. The ultrathin thickness of the films was corroborated by SEM, the average value measured for the 50 : 50 nanomembranes produced using 3000 rpm being 19 nm (Fig. 7b).

Conductivity measurements

The electrical properties of the nanomembranes were studied on an insulating substrate using a Keithley 6430 Sourcemeter. The conductivity determined for the P3TMA:PE44 80 : 20 nanomembranes ranged from $\sim 10^{-4}$ to $\sim 10^{-5}$ S cm^{-1}, depending on the thickness. These values are within the range typically found for semiconductor polythiophene derivatives bearing carboxylate groups.[28,29] Thus, the carboxylate side groups affect the electron transport through the π-conjugated backbone of the polymer. Unfortunately, measurements for the 50 : 50 and 20 : 80 were not possible indicating that the conductivity decreases when the concentration of P3TMA reduces.

Degradation studies

Enzymatic degradation studies of P3TMA:PE44 blends with Lipase PS, which was reported to degrade very efficiently aliphatic polyester films,[30] indicate that the degradation of nanomembranes starts after one week. More specifically, the appearance of thin grooves in the surface (Fig. 8a) was observed after seven days of exposure under enzymatic degradation conditions. After two additional weeks, the thin grooves transform into large and/or deep cracks, like those displayed in Fig. 8b and c. This produces the detachment of the P3TMA domains and the solubilization in the medium of the low molecular weight products arising from the polyester. On the other hand, nanomembranes made exclusively of P3TMA did not undergo any enzymatic degradation after four weeks but had a swelling effect due to the absorption of water from the medium, which produces very small cracks in the surface (Fig. 8d). This swelling effect should be attributed to the polar nature of the carboxylate substituents. These results demonstrate that the contribution of the polyester is crucial not only for the mechanical integrity of

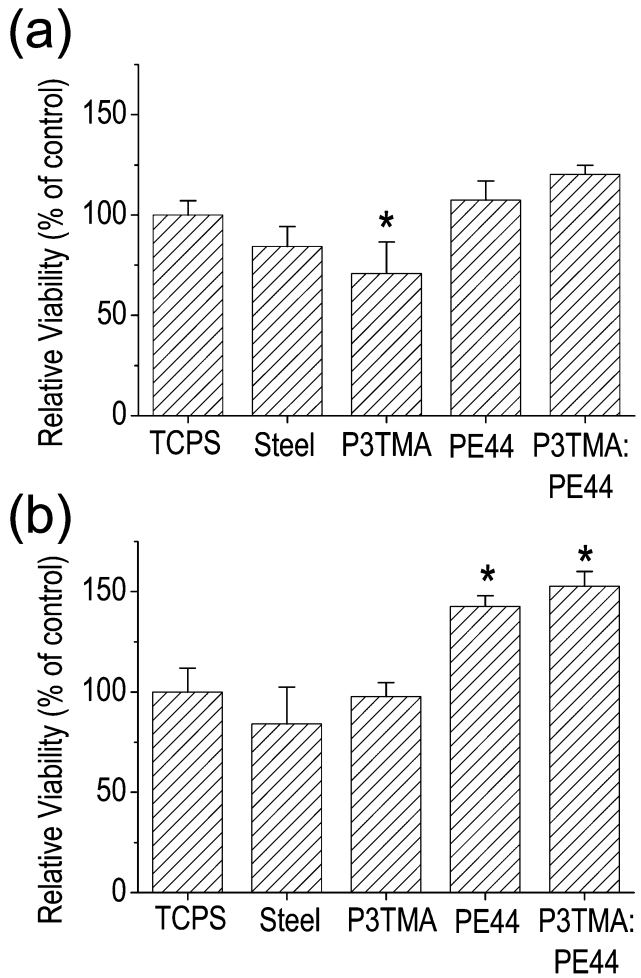

Fig. 9 Cellular adhesion (a) and cellular proliferation (b) on the nanomembranes. *$p < 0.05$ *vs.* TCPS. Five samples were analyzed for each group. Bars represent the mean ± standard deviation. The asterisk indicates a significant difference with the control, Tukey's test ($p < 0.05$).

P3TMA:PE44 50 : 50 nanomembranes but also for their biodegradability.

Cellular adhesion and proliferation

Biological assays have been performed considering the HEp-2 cell line of human epithelial morphology due to its highly adherent characteristics. A quantitative comparison between P3TMA, PE44 and P3TMA:PE44 50 : 50 nanomembranes as substrates for cellular adhesion and proliferation is displayed in Fig. 9. Five samples were analyzed for each group of nanomembranes, the standard deviation of the mean being small in all cases. Moreover, those cases in which the difference between the bioactive behaviour of the nanomembranes and the control TCPS plates is significant (confidence level of 95%) have been explicitly labelled in Fig. 9 with an asterisk. Cellular adhesion is significantly lower on P3TMA than on the control, tissue culture polystyrene (TCPS), while the adhesion on the polyester and P3TMA:PE44 is similar to that on the TCPS (Fig. 9a). After 7 days of culture in identical conditions, examination of the cellular viability shows a remarkable enlargement in the number

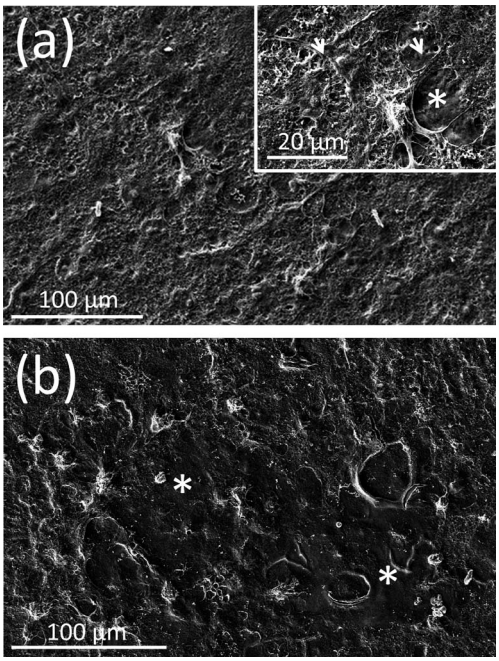

Fig. 10 Micrographs of the HEp-2 cells cultured for seven days on the surfaces of the (a) P3TMA:PE44 50 : 50 and (b) individual P3TMA nanomembranes. Morphological details of the cellular adhesion (arrows) are displayed in the inset of (a). The asterisks indicate domains at the surface without cells.

of viable cells onto the PE44 and P3TMA:PE44 50 : 50 films but not onto the P3TMA substrate (Fig. 9b).

The SEM micrograph displayed in Fig. 10a shows the characteristics of cells cultured onto the surface of hybrid P3TMA:PE44 nanomembranes. As it can be seen, a cellular monolayer with cells having a broad spreading was formed on the surface, even though very small domains without cells are occasionally detected (see the inset of Fig. 10a). In contrast, relatively large microdomains without cells are frequently identified on the surface of P3TMA, as is reflected in the SEM micrograph displayed in Fig. 10b. These observations suggest that, although the receptivity of the P3TMA surface to cellular adhesion is relatively poor, colonization of such material through proliferation of the adhered cells should be possible by considering more days of culture. Indeed, the biological behavior of P3TMA has been found to be worse than that observed for other polythiophene derivatives with higher conductivities and doping levels, *e.g.* poly (3,4-ethylenedioxythiophene).[11,16]

In spite of the limitations of this CP to allow cell attachment, the P3TMA:PE44 50 : 50 blend has been identified as a potent cellular matrix showing the highest viability to support the cellular adhesion and proliferation. Thus, although the use of polyesters as biomaterials with biomedical applications is broadly accepted due to its very high biocompatibility, the combination of PE44 with the CP has allowed us to improve the behaviour of such polyester as bioactive platform. It should be noted that cell attachment to CPs, especially to polythiophene derivatives, has been found to be favoured because of the following two reasons:[11,16] (1) the morphology of these materials is suitable to establish an intimate interfacial contact with cells; and (2) the exchange of anions between the CP and the cells

through the cellular membrane. Moreover, although polythiophene derivatives are usually biocompatible materials, monomers retained in the polymeric matrix are cytotoxic.[11] According to these observations, the poor bioactivity of P3MTA has been attributed to the toxicity of the 3MTA monomer, such damaging effect being minimized in the 50 : 50 blend. Thus, the reduction in the relative concentration of P3TMA to a half should be enough not only to eliminate the injurious effect of 3TMA but also to take advantage of the morphological and anion-diffusion benefits typically associated with CPs (*i.e.* promoting the bioactivity of the blend with respect to the polyester).

Conclusions

The present work presents the fabrication of very stable free-standing nanomembranes by combining a polythiophene derivative bearing carboxylate substituents in the 3-position of the heterocyclic ring and a biodegradable polyester. The thickness and roughness, which are controlled through the spin-coater speed, of the nanomembranes with 50 : 50 molar ratios obtained using a speed of 3000 rpm were smaller than 19 and 5 nm, respectively. The dimensions of these flexible films are only limited by the size of substrate used in the fabrication process. Although P3TMA:PE44 nanomembranes combine the semiconducting and biodegradable properties of the individual components, the cellular growth has been found to be higher for the blend than for the individual P3TMA and PE44. These results indicate that P3TMA:PE44 nanomembranes are potential candidates for the fabrication of electroactive scaffolds with biomedical applications. Thus, the superior ability of the P3TMA:PE44 blend to support the cellular adhesion and proliferation validates the utility of the biodegradable free-standing nanomembranes as a bioactive platform with semiconducting response for tissue regeneration.

Acknowledgements

This work has been supported by MICINN and FEDER funds (MAT2009-09138 and MAT2009-11513) and by the DIUE of the Generalitat de Catalunya (2009SGR925, 2009SGR1208 and XRQTC). We are indebted to Mr David Aradilla for his assistance in AFM analyses. A.G. acknowledges financial support from the Euro Brazilian Windows agency (grant no. 41309-EM-1-2008-PT-ERAMUNDUS-ECW-L16) for his 6-month stay at the UPC. M.M.P.-M. thanks financial support through a FPU-UPC grant. Support for the research of C.A. was received through the prize "ICREA Academia" for excellence in research funded by the Generalitat de Catalunya.

References

1 R. Vendamme, S.-Y. Onoue, A. Nakao and T. Kunitake, *Nat. Mater.*, 2006, **5**, 494.
2 R. Vendamme and T. Kunitake, *Soft Matter*, 2008, **4**, 797.
3 H. Watanabe, E. Muto, T. Ohzono, A. Nakao and T. Kunitake, *J. Mater. Chem.*, 2009, **19**, 2425.
4 H. Watanabe, T. Ohzono and T. Kunitake, *Macromolecules*, 2007, **40**, 1369–1371.
5 H. Watanabe and T. Kunitake, *Adv. Mater.*, 2007, **19**, 909.
6 L. Qui, W. H. Lee, X. Wang, J. S. Kim, J. A. Lim, D. Kwak, S. Lee and K. Cho, *Adv. Mater.*, 2009, **21**, 1349.
7 P. Liu, Y. Wu, H. Pan, B. S. Ong and S. Zhu, *Macromolecules*, 2010, **43**, 6368.
8 C.-D. Liu, C.-K. Huang, S.-Y. Wu, J.-L. Han and K.-H. Hsieh, *Polym. Int.*, 2010, **59**, 517.
9 M. E. Nicho, D. Peña-Salgado and P. Altuzar-Coello, *Thin Solid Films*, 2010, **518**, 1799.
10 Y. Li, K. G. Neoh, L. Cen and E.-T. Kang, *Biotechnol. Bioeng.*, 2003, **84**, 305.
11 L. del Valle, F. Estrany, E. Armelin, R. Oliver and C. Alemán, *Macromol. Biosci.*, 2008, **8**, 1144.
12 A. Kotwal and C. E. Schmidt, *Biomaterials*, 2001, **22**, 1055.
13 E. Smela, *Adv. Mater.*, 2003, **15**, 481.
14 J.-C. Vidal, E. García-Ruíz and J.-R. Castillo, *Microchim. Acta*, 2003, **143**, 93.
15 M. Martí, G. Fabregat, F. Estrany, C. Alemán and E. Armelin, *J. Mater. Chem.*, 2010, **20**, 10652.
16 L. J. del Valle, D. Aradilla, R. Oliver, F. Sepulcre, A. Gámez, E. Armelin, C. Alemán and F. Estrany, *Eur. Polym. J.*, 2007, **43**, 2342.
17 B. Kim, L. Chen, J. Gong and Y. Osada, *Macromolecules*, 1999, **32**, 3964.
18 T. Fujimaki, *Polym. Degrad. Stab.*, 1998, **30**, 209.
19 T. Mosmann, *J. Immunol. Methods*, 1983, **65**, 55.
20 D. J. Liaw, B. Y. Liaw, J. P. Gong and Y. Osada, *Synth. Met.*, 1999, **99**, 53.
21 E. Armelin, O. Bertran, F. Estrany, R. Salvatella and C. Alemán, *Eur. Polym. J.*, 2009, **45**, 2211.
22 O. Bertran, E. Armelin, F. Estrany, A. Gomes, J. Torras and C. Alemán, *J. Phys. Chem. B*, 2010, **114**, 6281.
23 O. Bertran, P. Pfeiffer, J. Torras, E. Armelin, F. Estrany and C. Alemán, *Polymer*, 2007, **48**, 6955.
24 E. S. Yoo and S. S. Im, *J. Polym. Sci., Part B: Polym. Phys.*, 1999, **37**, 1357.
25 H. E. Kissinger, *Anal. Chem.*, 1957, **29**, 1702.
26 N. Sbirrazzuoli, Y. Girault and L. Elégant, *Thermochim. Acta*, 1997, **293**, 25.
27 S. Vyazovkin and N. Sbirrazzuoli, *Macromol. Rapid Commun.*, 2006, **27**, 1515.
28 F. Zang and M. P. Srinivivasan, *Macromol. Chem. Phys.*, 2008, **112**, 223.
29 K. H. Hsieh, K. S. Ho, Y. Z. Wang, S. D. Ko and S. C. Fu, *Synth. Met.*, 2001, **123**, 217.
30 A. Hoshino and Y. Isono, *Biodegradation*, 2002, **13**, 141.

